Structure, Volume *24*

Supplemental Information

Crystal Structure and Conformational Change Mechanism of a Bacterial Nramp-Family Divalent Metal Transporter

Aaron T. Bozzi, Lukas B. Bane, Wilhelm A. Weihofen, Abhishek Singharoy, Eduardo R. Guillen, Hidde L. Ploegh, Klaus Schulten, and Rachelle Gaudet

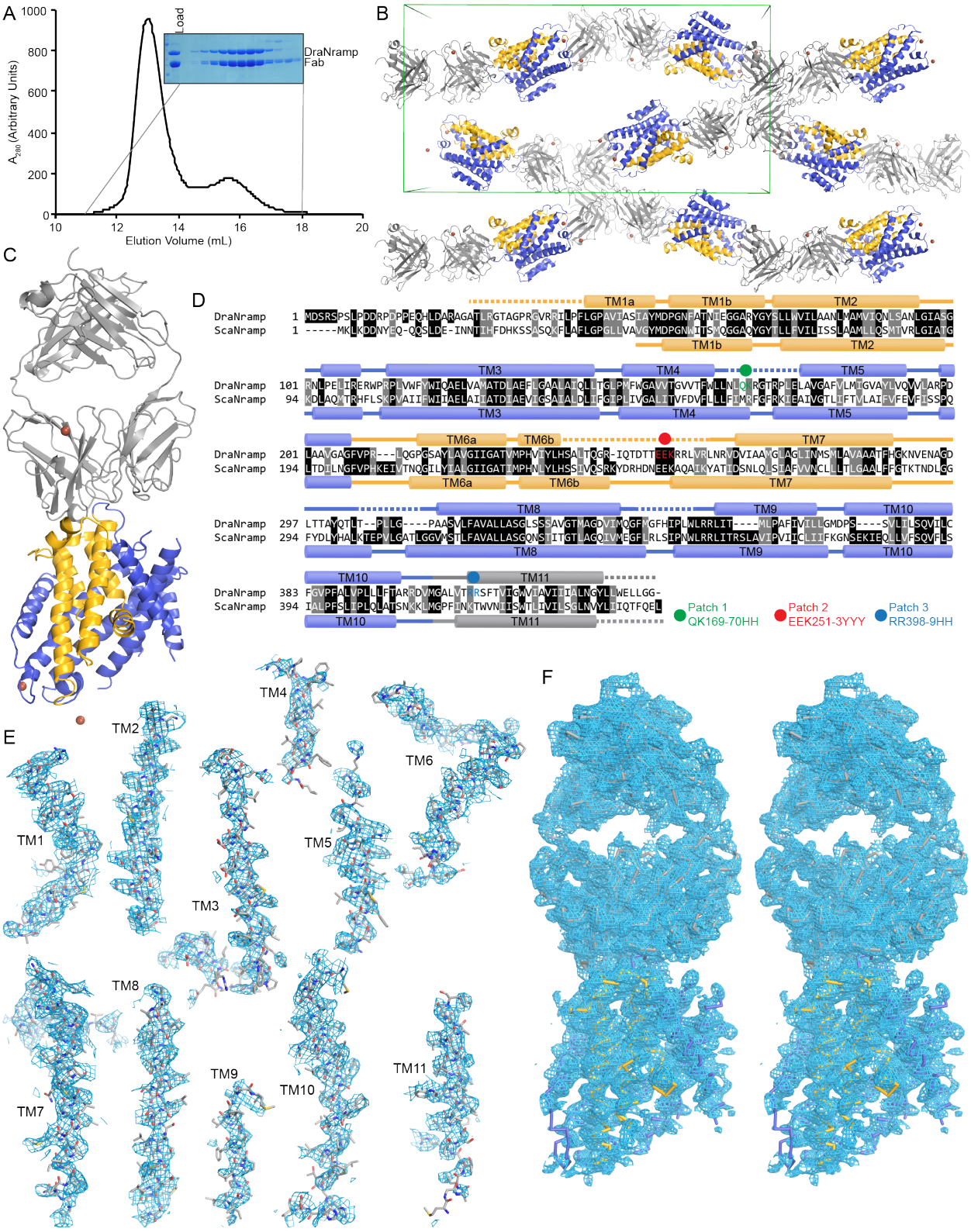

Figure S1, related to Figure 1. Crystal structure of DraNramp bound to a Fab. (A) SEC trace of 1:1.2 DraNramp-Fab mixture, and Coomassie-stained SDS-PAGE of the resulting fractions. (B) Crystal packing of DraNramp-Fab crystals. The Fab variable regions primarily bind extracellular loop 7-8, and crystal packing interactions involve Fab-Fab interfaces as well as an interaction between the Fab constant regions and DraNramp intracellular loops.

Unit cell is shown in green for scaling reference. (C) The asymmetric unit contains one DraNramp transporter (blue and yellow), one Fab (gray), and three osmium ions (ruby). (D) Sequence alignment of *Deinococcus radiodurans* (DraNramp) and *Staphylococcus capitis* (ScaNramp), with their secondary structure indicated above or below the sequence, respectively. The overall sequence identity is 38%. (E) Final $2F_o$-F_c electron density map contoured at 1σ and corresponding model in sticks representation for each transmembrane segment of DraNramp. (F) Stereo image of the final $2F_o$-F_c electron density map contoured at 1σ. In all panels except (E), the bundle (TM1, 2, 6, 7) is colored yellow and the scaffold is colored blue.

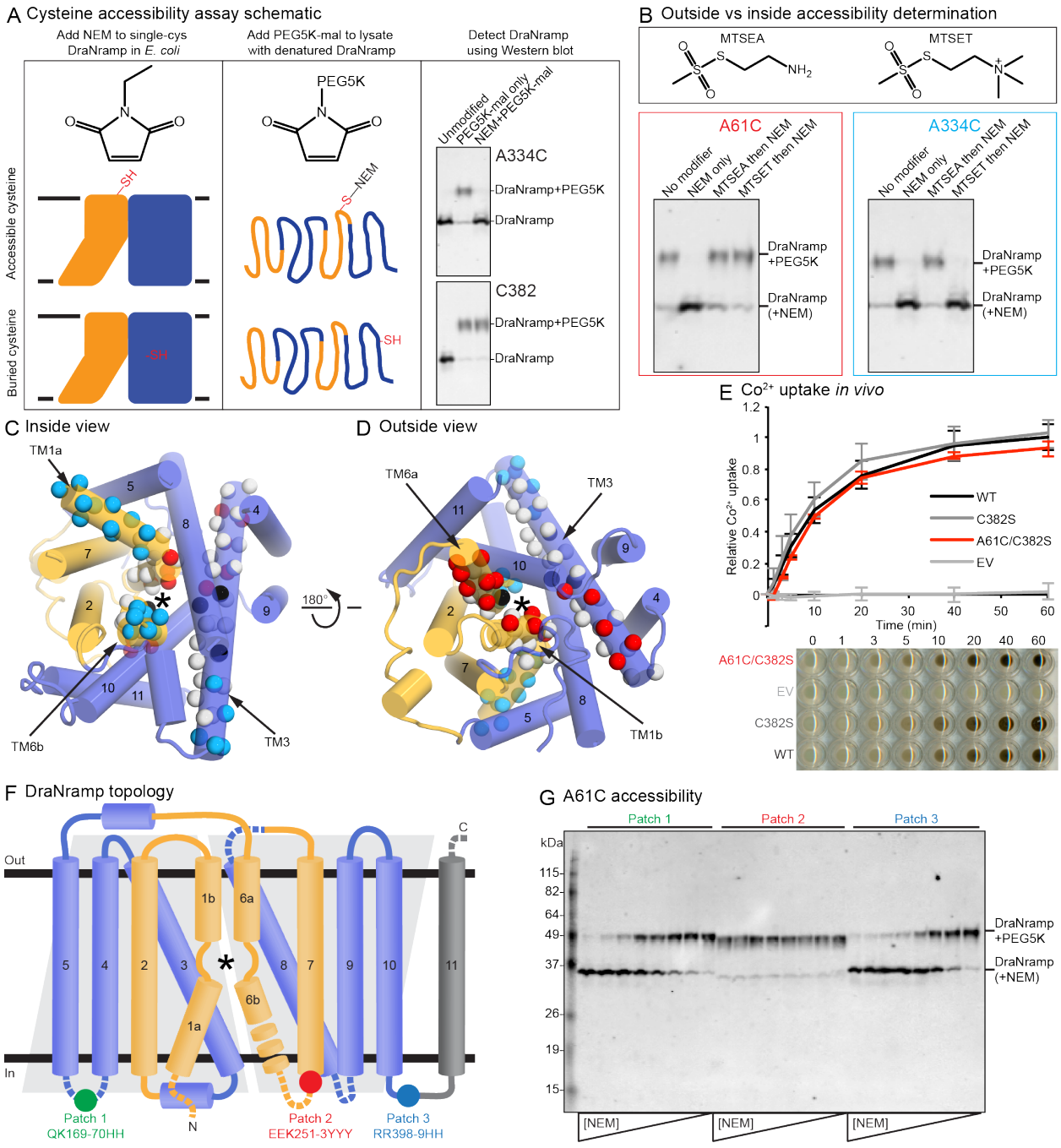

Figure S2, related to Figure 2. Cysteine accessibility and cobalt transport assays reveal location of outward metal permeation pathway. (A) For our *in vivo* cysteine accessibility assay, we added NEM to a panel of ~100 single-cysteine DraNramp mutants. Accessible cysteines (e.g. A334C) in the native protein react irreversibly with NEM, whereas buried cysteines (e.g. C382) do not. We then lyse the cells and denature the proteins in urea, sodium dodecyl sulfate, and dithiothreitol and add a maleimide derivative conjugated to PEG5K, which reacts with previously unmodified cysteines. We then use a Western blot for the N-terminal His-tag to observe a gel shift as a result of the PEG5K addition, which is prevented by reaction with NEM in the first step. By comparing the intensities of the lower and upper bands in the control case (PEG5K only) with their intensities when both NEM and PEG5K were added, we can determine the NEM-modified protein fraction. (B) The inner-membrane impermeable MTSET reagent allows us to determine whether accessible cysteines are modified from the cytosol or the periplasm. We add either MTSET or the similar but membrane-permeable MTSEA before adding NEM (thus blocking NEM

modification). However, these reagents form reversible disulfides that are cleaved by DTT in the denaturation step, thus allowing PEG5K-maleimide to react and observation of the upper band on the Western blot. For an outward-accessible position like A61C, both MTSEA and MTSET block NEM modification, whereas for an inward-accessible position like A334C, only MTSEA blocks NEM modification. (C,D) Cysteine-accessibility data from Table S1 plotted onto the DraNramp structure. View from the cytosol (C) showing the large cavity with inward-accessible positions (cyan spheres) that line the path to the metal-binding site (*).View from the periplasm (D) showing the outward-accessible positions (red spheres) that line the proposed metal permeation pathway to the binding site (*) in the alternate outward-open conformation. Black spheres were only accessible to NEM, and gray spheres were inaccessible to all modifiers. (E) *In vivo* Co^{2+} uptake assay allows comparison of the metal transport function of DraNramp mutants by measuring the pellet darkness (due to accumulated Co^{2+} precipitated as black solid CoS at the end of the assay). The A61C/C382S single-cysteine reporter mutant retains full activity. Data are averages ± s.d. ($n \geq 3$). (F) The three patch mutants made to our crystallization construct are located in the intracellular loops 4-5 (QK169-170HH), 6-7 (EEK251-253YYY), and 10-11 (RR398-399HH). The inverted repeat topology is indicated with light gray trapezoids, with the bundle and scaffold colored yellow and blue, respectively. The metal-binding site is marked (*), and loops disordered in the DraNramp structure are dashed. (G) We can assess the effect of mutations (such as the crystallization construct patch mutants) on NEM-modification of the A61C single-cysteine reporter across an NEM concentration gradient. For patch mutants 1 and 3, NEM modification reached completion at high NEM concentrations (complete elimination of the upper PEG5K band), with a slightly higher NEM concentration at midpoint for patch 1. For patch mutant 2, the lack of NEM modification at any tested concentration indicates this mutation causes A61C to be fully protected (buried), likely by locking the protein in the observed inward-facing conformation. A61C fractional modification data extracted from this Western blot are included in Figure 2D.

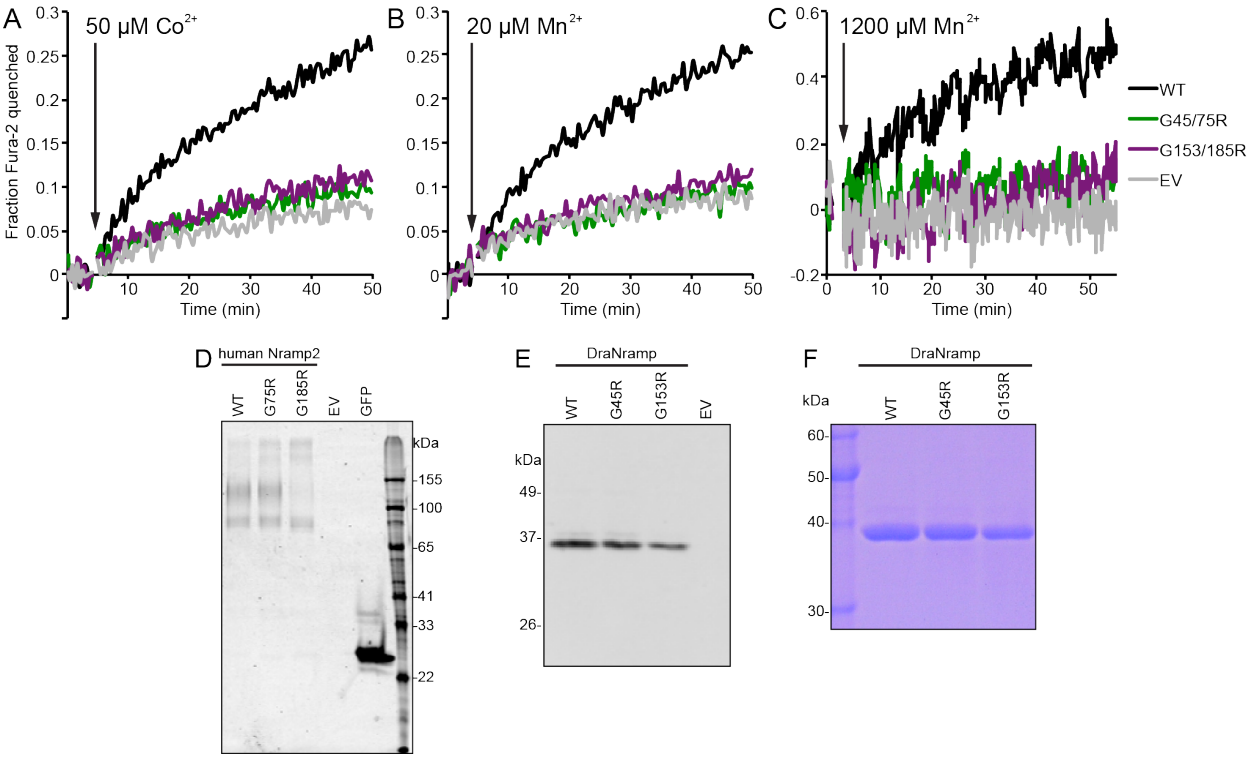

Figure S3, related to Figure 3. Loss of function glycine-to-arginine mutants are expressed for both human Nramp2 and DraNramp. (A-B) Transport of the transition metals Co^{2+} (A) and Mn^{2+} (B) in transfected HEK cells was monitored as quenching of Fura-2 fluorescence. Both G-to-R mutants exhibited severe loss of function (no transport activity above baseline) compared to WT human Nramp2 for both metals. Traces are representative of at least two independent transfection experiments. (C) We observed significant impairment of Mn^{2+} transport, monitored as quenching of Fura-2 fluorescence, with both G-to-R DraNramp mutants compared to WT when reconstituted into proteoliposomes. Traces are representative of three experiments. EV = empty vector/vesicle. (D) In-gel GFP fluorescence image of SDS-PAGE gel showing that C-terminally GFP-tagged G-to-R mutants both expressed in transfected HEK cells, although G185R expressed somewhat less. (E) Western blot, using an anti-His-tag antibody, showing that G-to-R DraNramp mutants both expressed although G153R expressed somewhat less. (F) Coomassie-stained SDS-PAGE gel of purified protein samples showing that both G-to-R DraNramp could readily be purified from *E. coli* membranes.

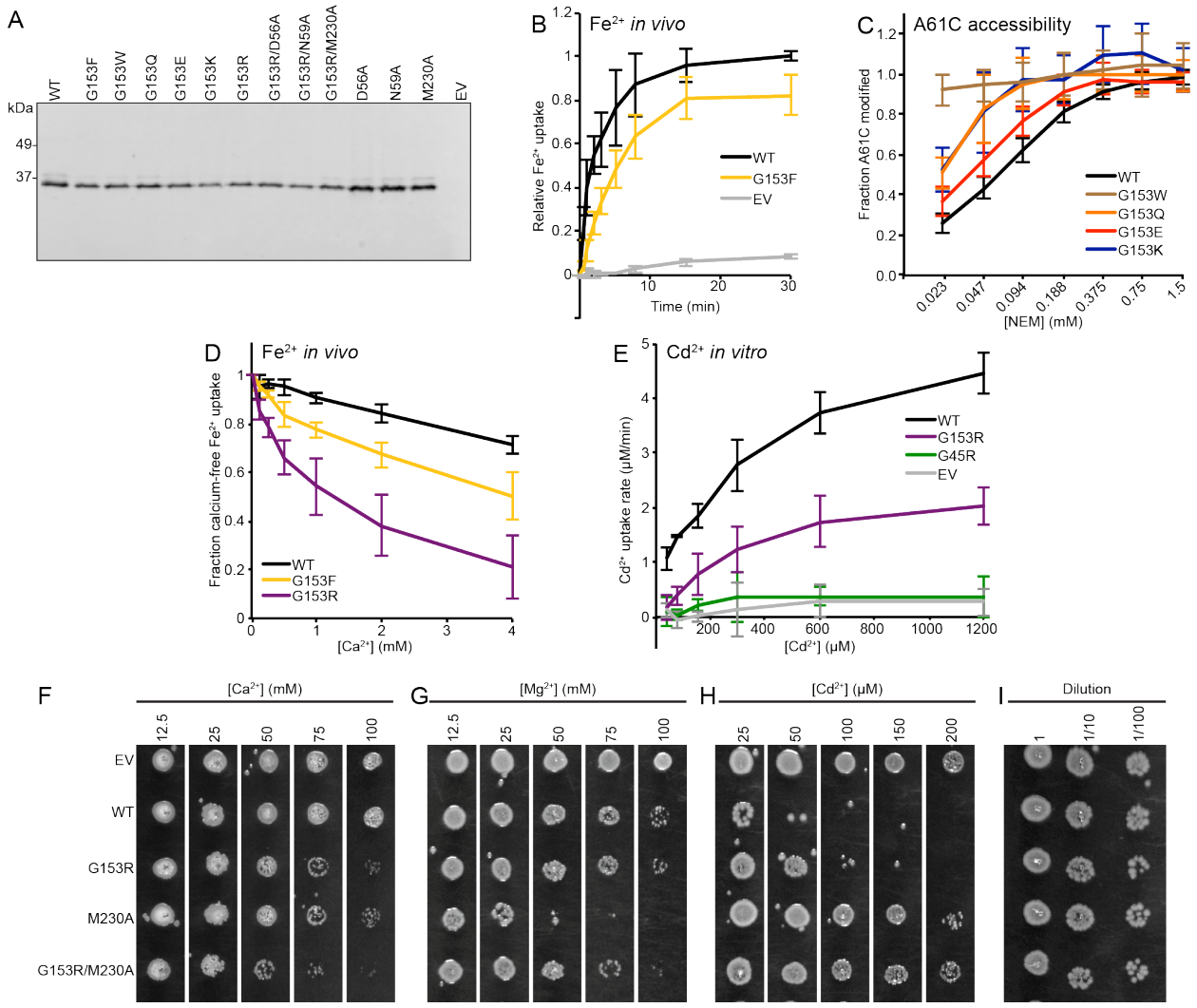

Figure S4, related to Figure 4. G153 mutations in DraNramp perturb outward-facing conformation and alter metal selectivity. (A) Western blot showing G153X mutants all expressed, but slightly less than WT. (B) G153F mutant exhibits slightly reduced *in vivo* Fe^{2+} transport. (C) All tested bulky substitutions at G153 increase the NEM-labeling rate of the A61C single-cysteine reporter, with G153F and G153W having the most dramatic effects. (D) Ca^{2+} competition reduces *in vivo* Fe^{2+} transport (15 min uptake in DraNramp-expressing *E. coli*) to a lesser degree for G153F than G153R, suggesting that the arginine perturbs the binding site in a manner particularly favorable to Ca^{2+}. WT and G153R data are reproduced from Figure 4E. (E) G153R impaired Cd^{2+} transport over a range of concentrations in an *in vitro* proteoliposome assay. Data are averages ± s.d. ($n \geq 3$). (F-I) Metal toxicity assessed using growth of DraNramp-expressing *E. coli* on LB-agar plates containing indicated metal concentrations (EV is empty vector control). (F) G153R increased sensitivity to Ca^{2+}, and G153R/M230A further increased sensitivity, suggesting synergistic perturbations to favor Ca^{2+} transport. (G) G153R did not increase Mg^{2+} toxicity, and G153R/M230A increased tolerance compared to M230A, suggesting that the G153R perturbation could be somewhat Ca^{2+} specific. (H) G153R enhanced Cd^{2+} tolerance less so than M230A. (I) Control serial dilutions on plates with no metal added. The gamma values were adjusted in the same manner for each condition to increase contrast between bacterial colonies and background. Growth trends are representative of three experiments.

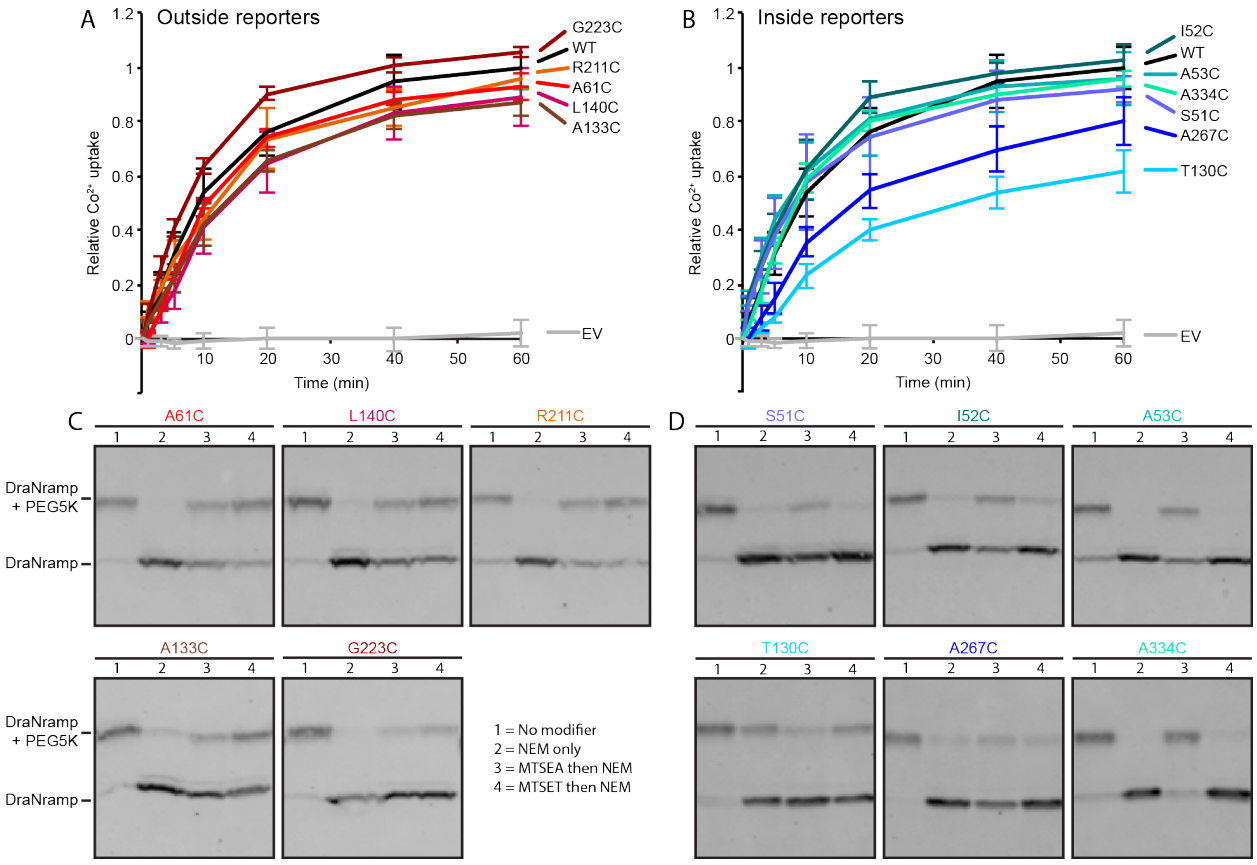

Figure S5, related to Figure 6. Inside and outside-accessible single-cysteine reporters preserve metal transport function. (A,B) *In vivo* Co^{2+} transport of outside (A) and inside (B) single-cysteine reporters. All mutants demonstrated significant activity, with only T130C and A267C showing some decrease below WT level. Data are averages ± s.d. ($n \geq 3$). (C,D) Solvent accessibility of outside (C) and inside (D) single-cysteine reporters using the membrane-impermeable cysteine modifier MTSET and the similar but membrane-permeable MTSEA, as described in Figure S2.

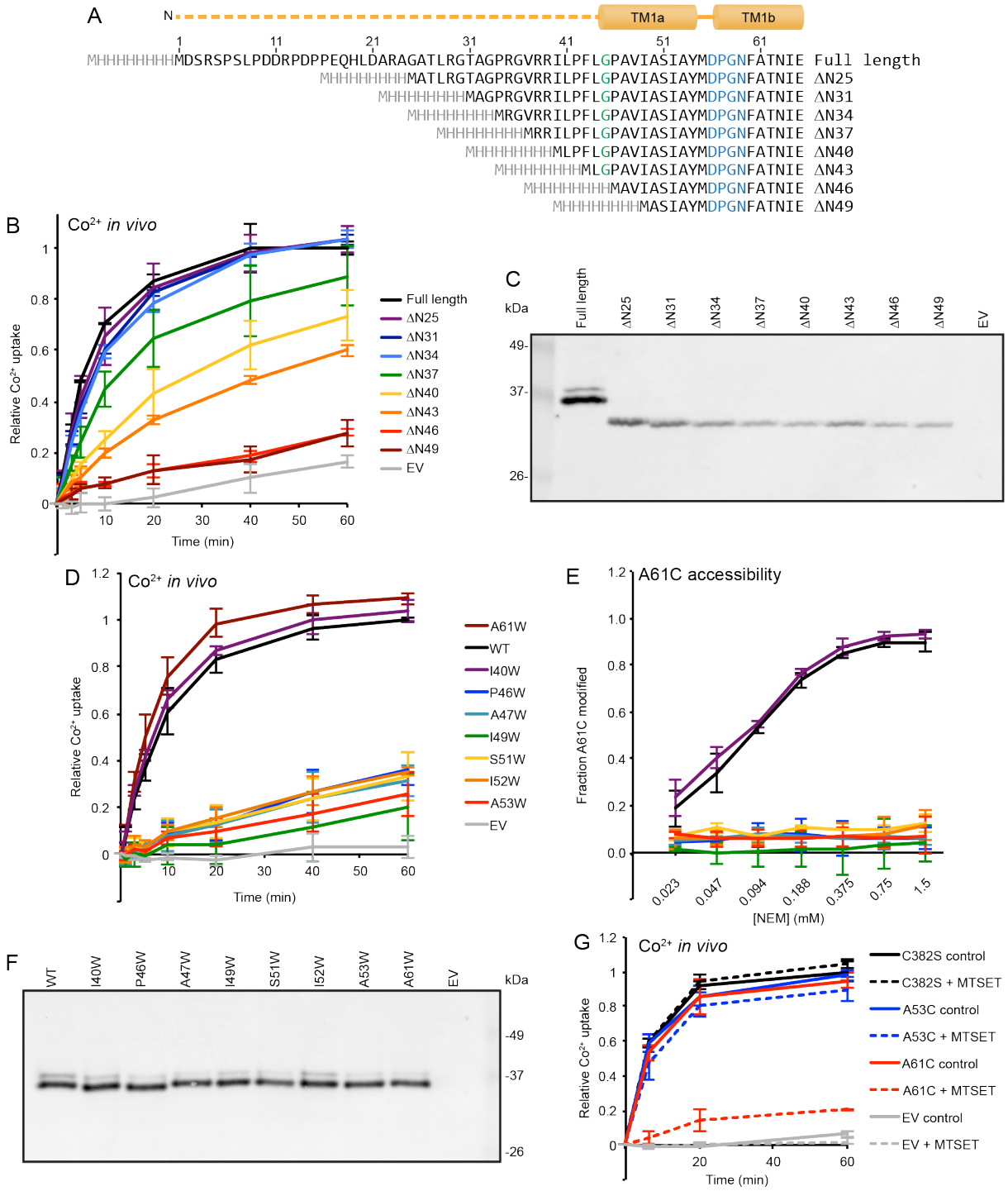

Figure S6, related to Figure 7. TM1a modification impairs DraNramp metal transport. (A) A series of N-terminal truncations removed from 25 to 49 residues while retaining the N-terminal 8His-tag (MHHHHHHHHH). (B) While ΔN25, ΔN31, and ΔN34 retained Co^{2+} uptake activity similar to full length DraNramp, ΔN37, ΔN40, and ΔN43 showed a gradual decrease in activity. ΔN46 and ΔN49, which both cut into TM1a, showed a severe loss of transport activity. Data are averages ± s.d. (n = 3). (C) Expression is reduced for N-terminal truncations compared to the full-length DraNramp as determined using a Western blot against the N-terminal His-tag. However, expression was similar for ΔN34 through ΔN49, although there were pronounced differences in transport activity. (D) Inserting tryptophans in place of residues P46, A47, I49, S51, I52, or A53 on TM1a inhibits Co^{2+} transport, while I40W

(preceding TM1a) does not. Interestingly, the TM1b A61W mutant retains full metal transport activity, consistent with the lack of impairment observed with NEM modification of A61C in Figure 7A, demonstrating that steric bulk can be accommodated in this position without impairing function. Data are averages ± s.d. (n = 3). (E) The six tested TM1a tryptophan mutations fully protected the A61C reporter from NEM modification, indicating that the proteins are locked in an inward-open state. The transport-capable I40W mutant showed WT-like A61C labeling. Data are averages ± s.d. (n = 4). (F) Western blot showing that all tested tryptophan mutants express similarly to WT DraNramp. (G) Pretreatment of A61C with the membrane impermeable, positively charged MTSET fully inhibits DraNramp Co^{2+} transport. The cysteine-less C382S and cytoplasmically-oriented A53C (and thus MTSET-inaccessible; Figure S5D) constructs are not significantly affected by MTSET pretreatment. Data are averages ± s.d. (n = 3).

Table S1, related to Figure 2. Cysteine accessibility results plotted on Figures 2A, S2C, and S2D

TM1			TM3			TM6		
Residue	Accessibility	Direction	Residue	Accessibility	Direction	Residue	Accessibility	Direction
E65	0.83	Outward	T146	0.48	--	S217	0.94	Outward
I64	0.35	--	L145	0.37	--	A218	0.94	Outward
N63	0.02	--	L144	0.85	Outward	Y219	0.89	Outward
T62	0.24	--	Q143	0.85	Outward	L220	0.90	Outward
A61	0.88	Outward	I142	0.12	--	A221	0.65	Outward
F60	0.10	--	A141	0.16	--	V222	0.09	--
N59	0.21	--	L140	0.90	Outward	G223	0.98	Outward
G58	0.87	Outward	A139	0.11	--	I224	0.75	Outward
P57	0.13	--	A138	0.12	--	I225	0.10	--
D56	0.92	Outward	G137	0.25	--	G226	0.06	--
M55	0.15	--	L136	0.80	Outward	A227	0.54	N.D.
Y54	0.36	--	F135	0.06	--	T228	0.14	--
A53	0.84	Inward	E134	0.18	--	V229	0.24	--
I52	0.82	Inward	A133	0.91	Outward	M230	0.95	Inward
S51	0.93	Inward	L132	0.15	--	P231	1.00	Inward
A50	0.99	Inward	D131	0.91	N.D.	H232	0.96	Inward
I49	0.91	Inward	T130	0.87	N.D.	V233	0.92	Inward
V48	0.94	Inward	A129	0.17	--	I234	0.95	Inward
A47	0.91	Inward	M128	0.25	--	Y235	0.98	Inward
P46	0.89	Inward	A127	0.19	--	L236	0.96	Inward
G45	0.75	Inward	V126	0.17	--	H237	0.95	Inward
L44	0.90	Inward	L125	0.20	--	S238	0.85	Inward
F43	0.74	Inward	E124	0.51	N.D.	A239	0.90	Inward
P42	0.84	Inward	A123	0.25	--	L240	0.90	Inward
L41	0.88	Inward	Q122	0.16	--	T241	0.75	Inward
I40	0.92	Inward	I121	0.25	--	Q242	0.80	Inward
			W120	0.76	Inward			
			Y119	0.12	--			
			F118	0.20	--			
			W117	0.92	Inward			
			V116	0.25	--			
			L115	0.75	Inward			
			P114	0.84	Inward			
			R113	0.94	Inward			

Supplemental Experimental Procedures

Cell-based metal uptake assays

E. coli cells expressing DraNramp (or an empty vector) were aliquoted 190 µL per well into 96-well round bottom plates at a density of OD_{600} = 5.26 in cobalt assay buffer (50 mM HEPES pH 7.3, 60 mM NaCl, 10 mM KCl, 0.5 mM $MgCl_2$, 0.217 % glucose). Transport was initiated by adding 10 µL of 4 mM $Co(NO_3)_2$ or freshly made 4 mM $FeSO_4$ + 4 mM ascorbic acid. For Ca^{2+} competition experiments, 10 µL of 20X concentrated $CaCl_2$ was added 1 min before Fe^{2+}. For NEM and MTSET pre-modification comparison experiments, cells were incubated with 3 mM NEM for 15 min at RT before cysteine quench or 3 mM MTSET for 30 min at 37°C and then washed twice. After the desired metal uptake time, excess EDTA was added to quench uptake and cells were washed thrice before adding 1% $(NH_4)_2S$ to precipitate internalized Co^{2+} or Fe^{2+}. Cells were pelleted, the supernatant was removed, the plates were scanned, and ImageJ64 was used to quantify the pellet darkness. End point (no metal-subtracted) darkness for WT DraNramp was set as 100% to determine relative transport abilities.

HEK293 cells were transfected with pCDNA3 containing human Nramp2 (with or without a C-terminal GFP tag) using Lipofectamine 2000 (Thermo Fisher) and incubated for 2 days at 30°C. Cells were loaded with Fura-2 AM and washed. A baseline fluorescence measurement (λ_{ex} = 380 nm; λ_{em}=510) was measured for ~3 min with 50 µL of pH 5.5 MES buffer, and then 25 µL of 3X metal was added to give final concentrations of 50 µM $Co(NO_3)_2$, 20 µM $FeSO_4$ + 20 µM ascorbic acid, 20 µM $MnCl_2$, or 20 µM $CdCl_2$ and fluorescence was measured for an additional 45 min. The fraction of the baseline fluorescence quenched was calculated for each timepoint, and for each mutant wells with similar baseline fluorescence values were used to generate the representative traces for each metal.

In vitro metal transport

Purified DraNramp was reconstituted into liposomes made from POPE, POPC, and POPG (Avanti Polar Lipids) in a 50:35:15 ratio by mixing 1:500 protein:lipid in a 5 mM DM solution and dialyzing for 3-4 days in 10 mM MOPS pH 7, 100 mM KCl. Liposomes were permeabilized using freeze-thaw cycles to load 100 µM Fura-2, extruded 21 times through a 400 nm filter, and separated from external dye using a PD10 column. Liposomes were diluted three-fold into 10 mM MOPS pH 7, 100 mM NaCl and baseline fluorescence measured, after which 50 nM valinomycin was added to establish a negative internal potential along with metal substrate ($CdCl_2$, $MnCl_2$, or $CaCl_2$). Fluorescence (l_{ex}=340 and 380 nm; l_{em}=510 nm) was monitored at RT for 45 min, before adding 0.25 µM ionomycin at 60 min to measure maximum signal. The intraliposome concentration of Cd^{2+} or Ca^{2+} was determined using: $[M^{2+}]_{inside} = ([M^{2+}]_{free}[Fura\text{-}2]_{total})/(K_D + [M^{2+}]_{free}) + [M^{2+}]_{free}$, where K_D is the K_D of the M^{2+} and Fura-2 (Cd^{2+} = 1 pM; Ca^{2+} = 135 nM) (Grynkiewicz et al., 1985; Hinkle et al., 1992) while relative fluorescence quenching (with post-ionomycin set to 100%) was determined for Mn^{2+}. Transport rates were determined by linear regression of the data for the first 5 min after Cd^{2+} addition and the first 30 min after Ca^{2+} addition.

Toxicity assay

Plates containing indicated concentrations of added $MgCl_2$, $CaCl_2$, or $CdCl_2$ were prepared by mixing 4 mL 10X metal with 36 mL LB-ampicillin-agar. Cells (1 µL at OD600=0.01 and additional serial dilutions on control plate) were plated 90 min post-induction and incubated overnight at 37°C. Plates were imaged on an AlphaImager system and gamma values were adjusted the same way for all images to increase contrast between colonies and the background agar.

Supplemental References

Grynkiewicz, G., Poenie, M., and Tsien, R.Y. (1985). A new generation of Ca^{2+} indicators with greatly improved fluorescence properties. J Biol Chem *260*, 3440-3450.

Hinkle, P.M., Shanshala, E.D., 2nd, and Nelson, E.J. (1992). Measurement of intracellular cadmium with fluorescent dyes. Further evidence for the role of calcium channels in cadmium uptake. J Biol Chem *267*, 25553-25559.